Journal of Biomedical Optics

SPIEDigitalLibrary.org/jbo

Label-free cell-based assay with spectral-domain optical coherence phase microscopy

Suho Ryu
Kyung-A Hyun
Jung Heo
Hyo-Il Jung
Chulmin Joo

SPIE

Label-free cell-based assay with spectral-domain optical coherence phase microscopy

Suho Ryu,[†] Kyung-A Hyun,[†] Jung Heo, Hyo-Il Jung, and Chulmin Joo[*]
Yonsei University, School of Mechanical Engineering, Seoul 120-749, Republic of Korea

Abstract. Quantitative measurement of dynamic responses of unstained living cells is of great importance in many applications ranging from investigation of fundamental cellular functions to drug discoveries. Conventional optical methods for label-free cell-based assay examine cellular structural changes proximal to sensor surfaces under external stimuli, but require dedicated nanostructure-patterned substrates for operation. Here, we present a quantitative imaging method, spectral-domain optical coherence phase microscopy (SD-OCPM), as a viable optical platform for label-free cell-based assay. The instrument is based on a low-coherence interferometric microscope that enables quantitative depth-resolved phase measurement of a transparent specimen with high phase stability. We demonstrate SD-OCPM measurement of dynamic responses of human breast cancer cells (MCF-7) to 2-picolinic acid (PA) and histamine. [DOI: 10.1117/1.JBO.19.4.046003]

Keywords: label-free; cell-based assay; spectral domain optical coherence phase microscopy; cell dynamics; cell biology.

Paper 130859R received Dec. 3, 2013; revised manuscript received Feb. 18, 2014; accepted for publication Mar. 10, 2014; published online Apr. 7, 2014.

1 Introduction

Monitoring cellular dynamics and behaviors under diverse conditions is of great importance to understand fundamental cell functions, and facilitates the development of novel cellular drugs. Conventional cell monitoring technologies[1] typically employ secondary contrast agents such as fluorescence dyes to visualize intracellular activities. However, labeling cells with the exogenous agents involves extra time and cost, and the agents may also perturb the intrinsic cellular functions.[2] Moreover, the labeled cells may not be suitable for longitudinal studies over long periods of time due to photobleaching and potential toxicity.[3]

Electrical impedance sensing (ECIS) has been investigated for label-free cell-based assay.[4] ECIS measures electrical impedance changes of metallic electrodes patterned on a substrate, on which cells adhere and interact. Upon external stimuli, the impedance changes reflect a myriad of cellular responses to drugs and pH/temperature dependence. Optical alternatives have also been developed. Commercial optical systems employ substrates patterned with resonant waveguide grating (RWG)[5] and photonic crystal structures[6] to measure changes of refractive index (RI) near the cell-substrate interface within ~200 nm. One notable application is measuring dynamic mass redistribution (DMR). DMR represents relocations of intracellular structures due to receptor activation or deactivation.[7] The main assumption is that the total amount of proteins is the same and spatial redistribution of intracellular structures is induced due to the stimulants.[7] The DMR process has been one of the main targets for cellular drug development, and therefore conventional label-free cell assay systems have focused on measuring the changes proximal to cell-substrate interface to measure local variation of RI, or the changes in accumulated intracellular mass. These methods have been utilized to examine various cell activities, such as proliferation, apoptosis, and G-protein-coupled receptor (GPCR) binding.[8]

Despite the attractive features, operation of these techniques requires dedicated substrates patterned with either metallic electrodes or nanostructures.[9] These surfaces are costly to fabricate, and the strategies for surface protection and functionalization are also required for proper cell adhesion. Therefore, the techniques capable of monitoring label-free cells with commercially available microtiter plates would facilitate cell-based research.[9]

Spectral-domain optical coherence phase microscopy (SD-OCPM)[10] is an optical microscopy technique capable of producing depth-resolved quantitative phase images of biological specimens. It is characterized by subnanometer level optical path-length sensitivity, and demonstrated dynamic measurement of antigen-antibody interactions.[11] Here, we demonstrate SD-OCPM as a viable platform for label-free cell-based assay, which can operate with commercial glass-bottom microtiter plates. We present its capability by measuring the responses of human breast cancer cells (MCF-7) to 2-picolinic acid and histamine.

2 Materials and Methods

2.1 *SD-OCPM Principle and Experimental Setup*

The operation of SD-OCPM is detailed elsewhere.[10] Figure 1 depicts SD-OCPM setup for label-free cell-based assay. A super-continuum laser (SC-400, Fianium Inc., Southampton, United Kingdom United Kingdom) passed through a long-pass filter (Chroma Inc., Bellows Falls, Vermont, HHQ550lp) and was directed to the fiber interferometer. Combined use of the long-pass filter and the single-mode fiber interferometer resulted in the sample light centered at ~800 nm with a full width at half maximum bandwidth of ~200 nm. The light from the sample arm fiber was collimated with a diameter of ~4.4 mm, and passed

*Address all correspondence to: Chulmin Joo, E-mail: cjoo@yonsei.ac.kr

[†]These authors contributed equally.

0091-3286/2014/$25.00

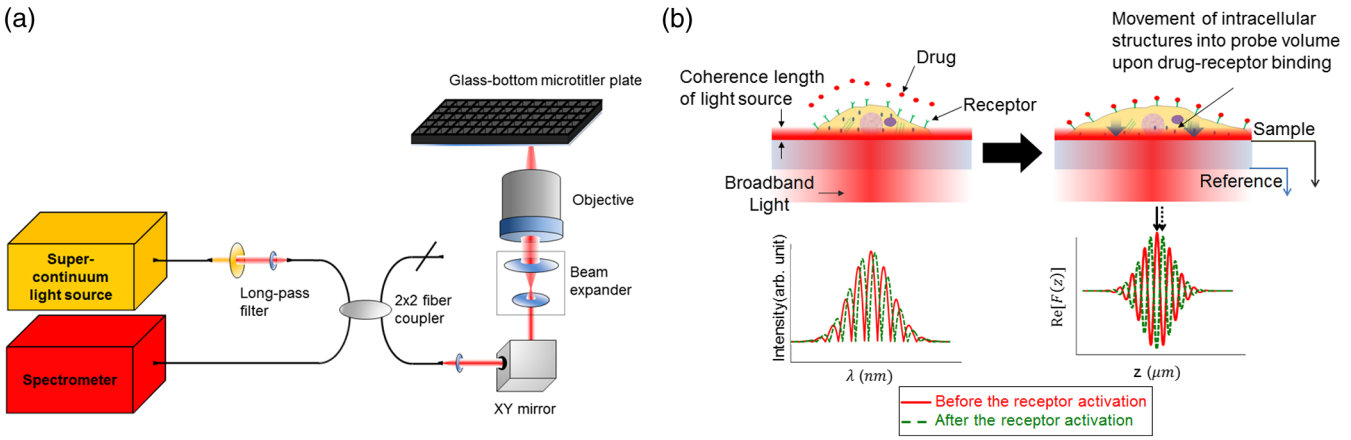

Fig. 1 (a) Experimental configuration of spectral-domain optical coherence phase microscopy (SD-OCPM) for cell assay. Light from a super-continuum laser was directed into a 2×2 fiber-based coupler. In the sample arm, the output beam was collimated, passed through a galvanometric beam scanner and subsequently was expanded by the beam expander. The expanded beam was then focused onto the cell-substrate interface. The reflected light was re-coupled into the fiber and detected by a spectrometer in the detection arm. (b) The back-reflected light from reference (bottom) and sample (top) surfaces interfere with each other to produce interference fringes. When the receptors on cell membrane are activated, relocation of intracellular structures proximal to the cell-substrate interface is induced, which results in a fringe shift in the interference spectrum (full-lined arrow to dashed arrow). Such fringe shifts can be quantified by examining the phase of the corresponding interference signal in the path-length resolved information.

through the two-dimensional galvanometric scanner (Thorlabs, Inc., Newton, New Jersey GVS-002). The beam was then focused on the top surface of a glass bottom microtiter plate with a focusing lens (Thorlabs, Inc., LSM05-BB). The light was reflected from the interfaces along the beam path, and re-coupled back into the interferometer. The interference signal was detected by a custom-built spectrometer at the detection arm with a maximum line rate of 70 kHz. The SD-OCPM was configured as an inverted microscope for live cell imaging.

The interference between the reflections from the top (measurement) and bottom (reference) surfaces of a substrate produces an interference spectrum as depicted in Fig. 1(b). As noted by Fang et al.[5] and in Schröder et al.,[7] upon activation of cell membrane receptors by external ligands, the cells undergo intracellular mass redistribution which results in alteration of cell adhesion and local scattering properties inside the cell. These changes proximal to the cell-substrate interface [red thick line on the substrate, Fig. 1(b)] lead to a fringe shift in the interference spectrum, which is in turn translated into the phase change in the optical path length domain. The coherence length of the light source determines the detection volume. In our setup, it was measured to be $\sim 1.4\ \mu$m in air, which is much smaller than the thickness of MCF-7. We performed confocal microscopy imaging of fluorescently labeled MCF-7s. The cells were labeled with PKH26 (Mini26, Sigma-Aldrich, St. Louis, Missouri) and were imaged by a confocal microscope ($63 \times /1.2$ NA, Zeiss LSM 510, Germany). The thickness of MCF-7 monolayer was measured to $\sim 12\ \mu$m on average. The fluctuations from other regions inside the cells would be rejected due to a short coherence length.

In this study, we set the lateral resolution to be $\sim 20\ \mu$m to measure averaged cellular responses over the entire well, while maintaining the ability to resolve individual cells. Higher spatial resolution can be readily achieved with high NA lenses, and would enable to examine heterogeneous cellular responses and intracellular dynamic responses with subcellular resolution. However, it would compromise the number of cells that can be measured for a given acquisition time. In terms of label-free cell assay, it is more advantageous to examine large population of cells under the introduction of chemicals to obtain robust and reliable cellular response. Therefore, lateral resolution was set to be $\sim 20\ \mu$m. We also cultured the cells with high confluency ($>75\%$) to minimize the empty regions, thereby performing more valid measurements over the field-of-view (FoV). SD-OCPM measurement averaged over the FoV therefore represents the collective responses of multiple cells due to the stimulants. The random dynamics such as cell membrane fluctuation would be averaged out by examining multitudes of cells.

2.2 *Data Analysis*

The measured interference spectra were transformed from wavelength to wavenumber space as described in Mujat et al.[12] Inverse Fourier transform of the spectrum results in path-length resolved complex-valued information of a specimen. We located the interference signal between the reflections of the top and bottom surfaces of the microtiter glass substrate and examined its complex-valued signal. It can be seen that our measurement is greatly influenced by the reflection from the top surface of a glass substrate. The contribution of the light scattered from cell bottom membrane and other intracellular structures would be significantly smaller compared with that from the glass substrate. In order to alleviate this signal leakage problem, we adopted the strategy described in Ellerbee and Izatt.[13] We subtracted the first image from the subsequent time-lapsed image sets, thereby measuring the changes due to cellular responses only. The amplitude and phase of the differential measurements were then averaged over the entire FoV and plotted to examine dynamic responses. A small phase drift over time was eliminated by referencing the measured phase distribution relative to the cell-free regions in the same image. The FoV of

SD-OCPM image was 3.3×3.3 mm^2 per well, and the image size was 500×500 pixels. The pixel rate was set to 10 kHz. The image acquisition was performed at every 2 min.

2.3 *Cell Preparation and Chemicals*

A breast carcinoma cell line (MCF-7) was used to assess the capability of SD-OCPM label-free cell-based assay. The cells were suspended in Roswell Park Memorial Institute medium (RPMI, GIBCO BRL, Gaithersburg, Maryland) at a fixed concentration of 1×10^5/ml. The 100 μl of the sample was loaded on glass bottom multiwell plates (In Vitro Scientific, Sunnyvale, California, P384-1.5H-N) and incubated for 24 h prior to experiment.

We employed 2-picolinic acid (PA, Sigma-Aldrich, St. Louis, Missouri, P42800) and histamine (Sigma-Aldrich, H7125) to induce cellular changes. 2-picolinic acid (PA), a pyridine compound with a carboxyl side chain, is known to interrupt cellular metabolism. It arrests the cell cycles on G_1, leading to prohibition of the cell proliferation or cell death.[14] On the other hand, histamine is an organic compound that regulates cell proliferation through stimulation of histamine receptors on the cell membrane.[15] The cellular responses to histamine have been investigated with other sensor technologies.[16]

The chemicals were prepared by serially diluting 1-M stock solutions of each chemical with phosphate-buffered saline solution to obtain the concentrations of 5.0, 12.5, 25.0 mM for PA, and 1, 3, 5 μM for histamine, respectively.

2.4 *Experiment Procedure*

For measurement, cell-loaded multiwell plates were placed on a custom-built SD-OCPM specimen stage. We acquired the image prior to the chemical injection as a reference. The responses of the PA-treated and histamine-treated cells were then recorded for 30 and 40 min, respectively, right after the introduction of the chemicals. Several wells in each measurement were untreated as controls.

3 Results

3.1 *System Stability*

Prior to measuring cellular responses to the chemicals, SD-OCPM performance was first evaluated. The microtiter well was filled with the incubation buffer, and the phase fluctuation of the interference signal between the reflections from the top and bottom surfaces of the glass substrate was recorded. The SD-OCPM beam was positioned stationary at the center of the FoV. The measured signal-to-noise ratio was ~50 dB, under which condition the theoretical sensitivity is ~2.2 mrad. The measured sensitivity in SD-OCPM was ~3.3 mrad in air. The difference between the theoretical and measured sensitivities may be due to the influence of external disturbances such as vibrations during the measurement.

We also performed SD-OCPM imaging of a cell-free substrate. A cell-free glass-bottom microtiter plate was initially filled with the incubation buffer, and the 5-μM histamine was injected at 1 min to examine the effect of bulk RI variation on the SD-OCPM phase measurement (indicated by an arrow in Fig. 2). As can be noted in Fig. 2, the histamine introduction did not produce a notable change. The standard deviations of the phase and intensity signals averaged over the entire FoV were found to be ~40.2 μrad and ~0.14, respectively. Unlike other optical cell-based assay technologies that measure the changes of RI proximal to the sensor surface, SD-OCPM measures the changes of optical thickness near the top surface of the substrate. Therefore, SD-OCPM is more immune to bulk RI variation, and rather sensitive to movement of scattering structures inside the probe volume.

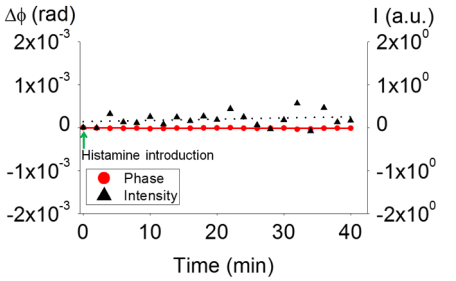

Fig. 2 Measured phase and intensity fluctuations for the cell-free plates. The chamber was initially filled with the incubation buffer and 5-μM histamine was injected at 1 min. The arrow indicates the time for the histamine injection. No notable changes were measured for the intensity and phase signals.

SD-OCPM signal fluctuations of untreated live cells were then measured (Fig. 3). Representative SD-OCPM images of the cells are also shown in Fig. 3. It can be noted that intensity values in the cell-free regions are larger than those in the regions on which the cells adhere. This can be explained by that the magnitudes of the reflected light in the cell-free regions are greater than other areas due to the larger RI gradient. The phase distribution in the SD-OCPM phase image represents the optical path-length delay due to cellular structures within the detection volume relative to the cell-free regions. The measured phase and intensity fluctuations exhibited small variations of ~427.1 μrad and ~0.2, respectively. Random cellular dynamics such as the intrinsic membrane motion within the probe volume may account for this small fluctuation.

3.2 *Measurement of Dynamic Cellular Responses*

Having evaluated the SD-OCPM performance, MCF-7 cell responses to 2-picolinic acid (PA) and histamine were measured. Representative SD-OCPM signals at a PA concentration of 12.5 mM are shown in Fig. 4(a), along with SD-OCPM intensity and phase images of the MCF-7s. It can be noted that the positive phase distributions that were initially observed at 0 min

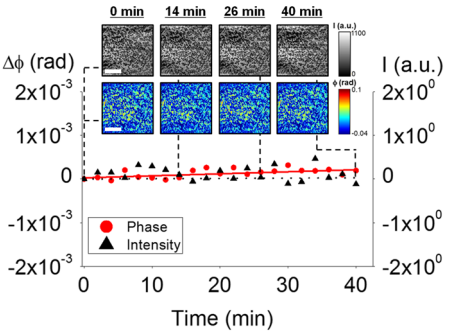

Fig. 3 Measured phase and intensity fluctuations for the live MCF-7 cells, along with representative SD-OCPM phase and intensity images. Small variations in the measured signals may be due to intrinsic cell membrane fluctuation and random motion of intracellular structures inside the probe volume. (Scale bar: 1 mm).

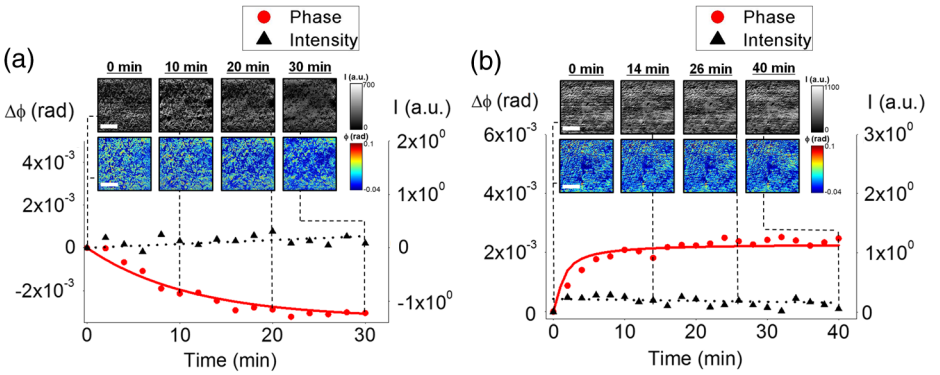

Fig. 4 Dynamic cellular responses measured with SD-OCPM. (a) Representative intensity and phase profiles for 12.5mM PA treated cells, along with the corresponding SD-OCPM images (Scale bar: 1 mm). Negative signal change can be observed in the phase signal, but no significant change was detected in the intensity measurement. (b) Representative intensity and phase measurements for 5 μM histamine treated cells. The representative SD-OCPM images are shown in the insets (Scale bar: 1 mm). The phase measurement presents a positive signal change in time, whereas the intensity measurement does not show a marked signal change.

decayed in time. This delay of the SD-OCPM phase signal may indicate a decrease in the number of cellular structures within the detection volume. Changes in the SD-OCPM intensity signal, on the other hand, were not significant. It may be due to that changes in the intensity signal were not larger compared with the power fluctuation of the light source. We separately performed bright-field microscopy imaging of the cells at the same concentrations, but found no marked changes (data not shown). This difference can be accounted for by that SD-OCPM measures the phase distribution only at the cell-substrate interface, while bright-field microscopy images are generated from the light transmitted through the cells. Hence, the bright-field microscopy would not be able to detect cell detachment and intracellular structural changes undergoing only at the cell-substrate interface.

Shown in Fig. 4(b) is SD-OCPM measurement of 5-μM histamine-treated MCF-7s. Representative SD-OCPM images of the cells can also be found in the insets. Although the changes were not pronounced as in the PA-treated cells, the averaged phase over the well increased and then became stabilized in 10 min. The cellular responses were heterogeneous at a single-cell level, but SD-OCPM measured increased cellular responses averaged over the entire well. SD-OCPM intensity signal, however did not show a marked change.

It can be seen that the SD-OCPM phase signal is more sensitive to small changes of cellular responses. The motion of intracellular structures was found to generate significant phase variations, and it has been used to measure viscoelastic properties inside the cells.[17] Joo and de Boer[18] have also measured the protein absorption and desorption on the glass substrate based on the phase variation.

We thus used SD-OCPM phase information to examine the cellular responses as a function of PA and histamine concentrations (Fig. 5). The higher PA concentration produced more rapid and large phase changes, while the control case did not exhibit a marked change [Fig. 5(a)]. Figure 5(b) shows the magnitudes of

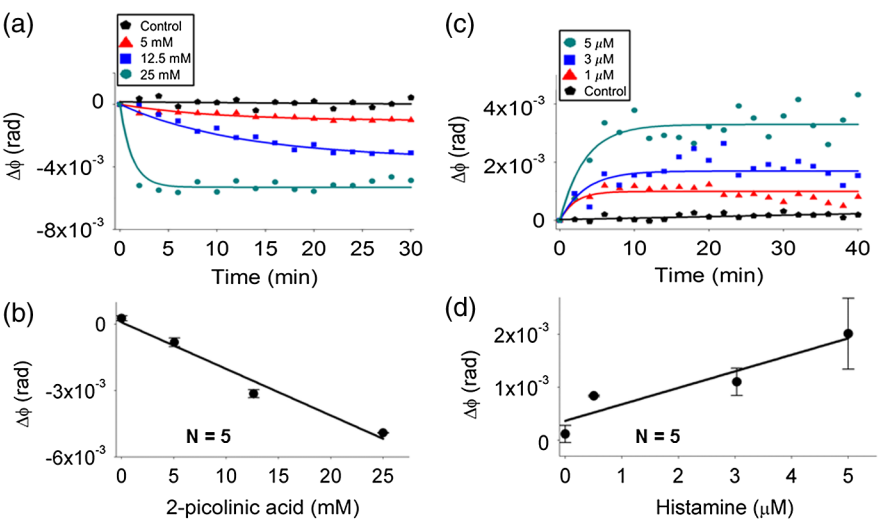

Fig. 5 (a) SD-OCPM phase measurements of 2-PA treated MCF-7s at different concentrations. (b) The averaged SD-OCPM phase change versus 2-PA concentration. (c) SD-OCPM phase measurements of histamine-treated MCF-7s at different concentrations. (d) The averaged SD-OCPM phase change versus histamine concentration. Five measurements were averaged for each concentration.

the phase changes averaged over five wells at each concentration. SD-OCPM phase changes were found to have a linear relationship with PA concentration as -210 μrad/mM [Fig. 5(b)]. Figures 5(c) and 5(d) show the representative cellular responses with different histamine concentrations and the phase changes averaged over five wells for each concentration. Large phase variations were observed at the higher histamine concentration. The SD-OCPM response against histamine concentration was found to vary linearly as $+390$ μrad/μM [Fig. 5(d)].

Our results with PA and histamine treated cells agree to earlier publications. Fernandez-Pol et al.[14] observed completed cell detachment and floating after ~48 h with the 3-mM PA treatment. Cytotoxicity of PA on human skin cells has also been reported.[19] Cell detachment and death result in a decrease in the optical thickness proximal to the substrate, which was detected as the negative phase changes in SD-OCPM measurement. SD-OCPM measurements with histamine treated MCF-7s are also consistent with the previous reports. For instance, Ferrie et al. measured the responses of human squamous carcinoma (A431) cells to histamine with the resonant waveguide optical sensor. They found the increased mass distribution proximal to substrate interface.[16] In addition, Brischwein et al.[20] utilized ECIS to measure the response of HELA cells to 25-μM histamine and observed an increased impedance signal, which was stabilized within 10 min.

In Figs. 4 and 5, exponential functions were used to fit the SD-OCPM phase signals in time. Temporal responses to the chemicals have previously been modeled with exponential functions. Malleo et al.[21] employed continuous differential impedance spectroscopy to examine HeLa cell responses to Polysorbate 20, and reported exponential behaviors in the measured signal as a function of time. Fang and Ferrie[22] have also observed the exponential signal changes for the A431 cells upon the introduction of various types of chemicals with RWG sensors. Our measurements with the PA and histamine exhibited similar behaviors. For the dependence of cellular responses on the histamine concentrations, we found the linear dependence of the cellular responses on the concentration ranges of 1 to 5 μM, which is consistent with other literatures. For example, Ferrie et al.[16] investigated the responses of A431 cells to histamine over the range of 2 nM to 100 μM, and observed a linear dependence on the histamine concentration in the range of 1 to 5 μM.

4 Discussion

The magnitudes and temporal profiles of SD-OCPM phase measurements can be utilized to evaluate efficacy of the drugs and to design the drugs with a desired performance. Such response can be a useful indicator for DMR occurrence, which represents activation or deactivation of membrane receptors, as demonstrated in Ref. 5. For example, Schröder et al.[7] have shown the real-time screening of GPCRs of cells against various types of drugs with RWG sensors.

Label-free cell-based assay with SD-OCPM exhibits several distinct advantages and drawbacks compared with the other optical methods.[23] It can operate with plain glass-bottom microtiter plates, which are commercially available and inexpensive compared with nanostructure-patterned plates. Moreover, since the measurement can be performed with transparent plain glasses, it can be easily integrated with other conventional microscopy technologies such as bright-field and phase contrast microscopes. Combination of SD-OCPM with other imaging modalities would allow for simultaneous quantitative label-free cell-based assay and direct visualization of cellular morphologies.

Its depth-resolved imaging capability based on low-coherence interferometry may also open up a new avenue for cellular studies. Recent investigations have shown that three-dimensional (3-D) imaging capability and high path-length sensitivity of SD-OCPM enabled measurement of nanoscale cell movement on subsecond scale. Bagnaninchi et al.[24] applied SD-OCPM to detect 3-D micromotion of stem cells in scaffolds by monitoring derivatives of measured phase information. Holmes et al.[25] have also demonstrated application of low-coherence interferometry for real-time cellular growth and viability monitoring in 3-D tissue scaffolds. Here, we demonstrated SD-OCPM as a label-free cell assay system capable of measuring DMR and cell adhesion/detachment based on its depth-resolved imaging ability.

Other quantitative phase imaging techniques have been developed to image unstained live cells. These include digital holographic microscopy,[26] Hilbert phase,[27] and Fourier phase imaging[28] techniques. These techniques provide high-contrast quantitative phase images of live cells in real-time. Yet, they operate on the light transmitted through the sample, and so cannot measure cellular changes at a specific depth. Here, our focus was on measuring DMR and cellular changes proximal to cell-substrate interface, which requires depth-resolved measurement capability.

As with other label-free interferometric techniques, SD-OCPM lacks of chemical specificity and specific structural information that leads to the measured signal. Researchers have employed multimodal techniques to understand the main contributors to the scattering signals inside the cells, and found that highly scattering structures such as mitochondria, cytoskeletons, and other subcellular structures are the main contributors in coherent imaging techniques.[29] Dynamic motion of intracellular structures inside the probe volume could lead to the measurable intensity and phase signals in SD-OCPM. The motion and accumulation of these structures led to phase variations, which have been used to measure viscoelastic properties inside the cells and to perform protein microassay.[17,18]

The scanning feature of SD-OCPM may also compromise the system stability and acquisition speed. The SD-OCPM phase noise due to mechanical scanning produced ~40.2-μrad noise level averaged over the FoV with the cell-free plates. Recent advances in high-speed wavelength-swept lasers and implementations of full-field optical coherence microscopes would enable high-speed, scan-less, and multiplexed OCPM cell measurement while achieving improved phase stability.[30,31]

5 Conclusion

We employed SD-OCPM to measure local phase variations proximal to cell-substrate within ~1.4 μm in depth to probe cell coverage and local intracellular dynamics. The setup is characterized by subnanometer level path-length sensitivity, and successfully monitored dynamic responses of MCF-7 cells to 2-picolinic acid and histamine. The intrinsic 3-D imaging capabilities of SD-OCPM are expected to provide a new dimension of investigation for cell studies. We believe that our present work extended the application of SD-OCPM to cell biology as a label-free cell assay system.

Acknowledgments

This research was supported in part by the research programs of National Research Foundation of Korea (NRF) (MEST No. NRF-2012R1A1A1003867) and Center for BioNano Health-Guard funded by the Ministry of Science, ICT & Future Planning (MSIP) of Korea as Global Frontier Project (H-GUARD_ 2013M3A6B2078959).

References

1. P. Pozarowski, E. Holden, and Z. Darzynkiewicz, "Laser Scanning Cytometry," in *Cell Imaging Techniques*, pp. 165–192, Springer, New York, NY (2006).
2. M. A. Cooper, "Optical biosensors in drug discovery," *Nat. Rev. Drug Discovery* **1**(7), 515–528 (2002).
3. S. M. Shamah and B. T. Cunningham, "Label-free cell-based assays using photonic crystal optical biosensors," *Analyst* **136**(6), 1090–1102 (2011).
4. I. Giaever and C. R. Keese, "A morphological biosensor for mammalian cells," *Nature* **366**(6455), 591–592 (1993).
5. Y. Fang et al., "Characteristics of dynamic mass redistribution of epidermal growth factor receptor signaling in living cells measured with label-free optical biosensors," *Anal. Chem.* **77**(17), 5720–5725 (2005).
6. B. T. Cunningham et al., "Label-free assays on the BIND system," *J. Biomol. Screening* **9**(6), 481–490 (2004).
7. R. Schröder et al., "Applying label-free dynamic mass redistribution technology to frame signaling of G protein-coupled receptors noninvasively in living cells," *Nat. Protocols* **6**(11), 1748–1760 (2011).
8. Y. Fang, A. G. Frutos, and R. Verklereen, "Label-free cell-based assays for GPCR screening," *Comb. Chem. High Throughput Screening* **11**(5), 357–369 (2008).
9. P. H. Lee, "Label-free optical biosensor: a tool for G protein-coupled receptors pharmacology profiling and inverse agonists identification," *J. Recept. Signal Transduction* **29**(3–4), 146–153 (2009).
10. C. Joo et al., "Spectral-domain optical coherence phase microscopy for quantitative phase-contrast imaging," *Opt. Lett.* **30**(16), 2131–2133 (2005).
11. C. Joo et al., "Spectral-domain optical coherence phase microscopy for label-free multiplexed protein microarray assay," *Biosens. Bioelectron.* **25**(2), 275–281 (2009).
12. M. Mujat et al., "Autocalibration of spectral-domain optical coherence tomography spectrometers for in vivo quantitative retinal nerve fiber layer birefringence determination," *J. Biomed. Opt.* **12**(4), 041205 (2007).
13. A. K. Ellerbee and J. A. Izatt, "Phase retrieval in low-coherence interferometric microscopy," *Opt. Lett.* **32**(4), 388–390 (2007).
14. J. Fernandez-Pol, V. H. Bono, and G. S. Johnson, "Control of growth by picolinic acid: Differential response of normal and transformed cells," *Proc. Natl. Acad. Sci.* **74**(7), 2889–2893 (1977).
15. V. A. Medina and E. S. Rivera, "Histamine receptors and cancer pharmacology," *Br. J. Pharmacol.* **161**(4), 755–767 (2010).
16. A. M. Ferrie, Q. Wu, and Y. Fang, "Resonant waveguide grating imager for live cell sensing," *Appl. Phys. Lett.* **97**(22), 223704 (2010).
17. C. Joo et al., "Diffusive and directional intracellular dynamics measured by field-based dynamic light scattering," *Opt. Express* **18**(3), 2858–2871 (2010).
18. C. Joo and J. F. de Boer, "Spectral-domain optical coherence reflectometric sensor for highly sensitive molecular detection," *Opt. Lett.* **32**(16), 2426–2428 (2007).
19. J. Fernandez-Pol, D. J. Klos, and P. D. Hamilton, "Antiviral, cytotoxic and apoptotic activities of picolinic acid on human immunodeficiency virus-1 and human herpes simplex virus-2 infected cells," *Anticancer Res.* **21**(6A), 3773–3776 (2001).
20. M. Brischwein et al., "Electric cell-substrate impedance sensing with screen printed electrode structures," *Lab on a Chip* **6**(6), 819–822 (2006).
21. D. Malleo et al., "Continuous differential impedance spectroscopy of single cells," *Microfluid. Nanofluid.* **9**(2–3), 191–198 (2010).
22. Y. Fang and A. M. Ferrie, "Label-free optical biosensor for ligand-directed functional selectivity acting on β_2 adrenoceptor in living cells," *FEBS Lett.* **582**(5), 558–564 (2008).
23. A. M. Ferrie et al., "High resolution resonant waveguide grating imager for cell cluster analysis under physiological condition," *Appl. Phys. Lett.* **100**(22), 223701 (2012).
24. P. O. Bagnaninchi et al., "Two-dimensional and three-dimensional viability measurements of adult stem cells with optical coherence phase microscopy," *J. Biomed. Opt.* **16**(8), 086003 (2011).
25. C. Holmes, M. Tabrizian, and P. O. Bagnaninchi, "Motility imaging via optical coherence phase microscopy enables label-free monitoring of tissue growth and viability in 3D tissue-engineering scaffolds," *J. Tissue Eng. Regener. Med.* (2013).
26. J. Kühn et al., "Label-free cytotoxicity screening assay by digital holographic microscopy," *Assay Drug Dev. Technol.* **11**(2), 101–107 (2013).
27. G. Popescu et al., "Erythrocyte structure and dynamics quantified by Hilbert phase microscopy," *J. Biomed. Opt.* **10**(6), 060503 (2005).
28. N. Lue et al., "Quantitative phase imaging of live cells using fast Fourier phase microscopy," *Appl. Opt.* **46**(10), 1836–1842 (2007).
29. S. Tang et al., "Imaging subcellular scattering contrast by using combined optical coherence and multiphoton microscopy," *Opt. Lett.* **32**(5), 503–505 (2007).
30. M. V. Sarunic, S. Weinberg, and J. A. Izatt, "Full-field swept-source phase microscopy," *Opt. Lett.* **31**(10), 1462–1464 (2006).
31. R. Huber, M. Wojtkowski, and J. Fujimoto, "Fourier domain mode locking (FDML): a new laser operating regime and applications for optical coherence tomography," *Opt. Express* **14**(8), 3225–3237 (2006).

Biographies of the authors are not available.